ACS APPLIED MATERIALS & INTERFACES

Research Article

www.acsami.org

Silicon Oxide Nanowires: Facile and Controlled Large Area Fabrication of Vertically Oriented Silicon Oxide Nanowires for Photoluminescence and Sensor Applications

Taiwo R. Alabi,[†] Dajun Yuan,[‡] David Bucknall,[†] and Suman Das*[,†,‡]

[†]School of Materials Science and Engineering, Georgia Institute of Technology, Atlanta, Georgia 30332, United States

[‡]Woodruff School of Mechanical Engineering, Georgia Institute of Technology, Atlanta, Georgia 30332, United States

Supporting Information

ABSTRACT: We describe a technique for the fabrication of dense and patterned arrays of aligned silicon oxide nanowires for applications in surface modification, optoelectronic, and electromechanical based devices. Conventional techniques for the fabrication of silicon oxide nanowires based on the vapor−liquid−solid (VLS) chemical vapor deposition (CVD) processes involve the use of high temperatures and catalysts. We demonstrate a technique that extends the use of a plasma thermal reactive ion etching for the fabrication of aligned silicon oxide nanowires with aspect ratios extending up to 20 and lengths exceeding 1 μm. The process incorporates phase separated PS-b-P4VP block copolymer loaded with an iron salt. The iron salt preferentially segregates into the P4VP layer and during an O_2 etch is not removed but forms a hexagonally packed array on the silicon oxide substrate. Further etching with CHF_3/O_2 gas mixture over time can generate nanodots, to nanopillars, and then nanowires of silicon oxide. The photoluminescence property of the as-fabricated nanowire arrays as well as the parasitic ferromagnetic effect from the iron oxide-tipped section of the wires resulting in coalescence under an scanning electron microscope (SEM) are demonstrated. This technique is simpler compared to existing VLS fabrication approaches and can be used for the direct fabrication of patterned arrays of nanowires when a laser interference ablation step is incorporated into the fabrication procedure.

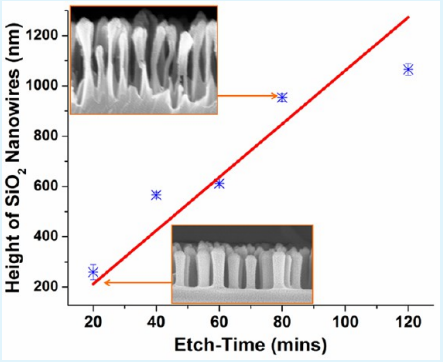

KEYWORDS: *silicon oxide nanowires, nanofabrication, reactive ion etching, photoluminescence, electromechanical sensor*

INTRODUCTION

The unique physical properties of one-dimensional (1D) nanomaterials have continued to generate interest among scientific researchers for years. Quantum confinement in 1D nanomaterials can generate size dependent excitation and emission of specific wavelengths of light;[1] it can also result in increased or ballistic transport properties in these nanomaterials.[2] Other effects include changes in the band gap energy that can lead to insulator−metal transitions and vice versa.[3] Unique properties resulting from quantum confinement have been utilized in the fabrication of optoelectronic,[4] electromechanical, optical,[5] photovoltaic,[6,7] and sensor[8] nanodevices.

There have been reports on the fabrication of 1D nanofeatures from a number of materials including ZnO,[9] TiO_2,[10−12] Pd,[13] Si,[14−16] Ge,[17−19] SiO_2,[20−22] carbon,[2,23] and indium phosphide.[24,25] Of all these 1D nanofeatures, nanowires made from silicon and silicon oxide, the most abundant material in the earth's crust, should primarily be the most accessible, integrable, and easy-to-fabricate.

Silicon oxide nanowires have been gaining continued interest in the literature due to some unique band gap properties that lead to blue light photoluminescence,[26] localization of light, near-field optical effects, as well as low-dimensional waveguiding. However, one of the problems plaguing the direct application of 1D nanofeatures, including silicon oxide nanowires, for device fabrication is the harsh processing conditions used for the fabrication of the nanowires.[27] The vapor liquid solid (VLS) fabrication technique,[21,28,29] for silicon oxide nanowire fabrication, uses temperatures greater than 800 °C, which makes the process not only expensive but also limits the type of supporting substrates that can be used to fabricate such features. Moreover, other low temperature fabrication techniques[30−32] have not been successful in fabricating high aspect ratio, aligned silicon oxide nanowires.

In addition, recent reports on the fabrication of high aspect ratio silicon nanowires involve not only multiple processing steps but also the use of hydrofluoric acid, a highly toxic and corrosive reagent.[33,34] Other "dry" fabrication techniques that do not involve the use of solvents[35] involve multiple steps including the deposition and phase separation of a block copolymer layer, argon/oxygen reactive ion etching, atomic layer deposition of alumina, oxygen etching, and silicon oxide/silicon etching. The multiple processing steps, with alumina serving as a hard mask, make the fabrication of patterned arrays

Received: May 12, 2013
Accepted: August 5, 2013
Published: August 5, 2013

   dx.doi.org/10.1021/am401787c | ACS Appl. Mater. Interfaces 2013, 5, 8932−8938

of silicon or silicon oxide nanowires using "dry" fabrication techniques almost impossible. Furthermore, the as-fabricated silicon/silicon oxide nanowires have a low aspect ratio with a 127 nm maximum height.

A very recent report has demonstrated the ability to fabricate silicon nanowires using a dry, hard mask fabrication approach.[36] Although the technique appears to be robust, the maximum height of the as-fabricated silicon nanowires is only ~500 nm, and the approach does not provide a means for the direct patterning of the silicon nanowires.

The ideal fabrication process for silicon oxide nanowires should not only allow easy integration with current technologies used in the electronics industry, but should also be robust enough to accommodate specifications for various patterns, and aspect ratios of nanowires for different applications.

We report a top-down fabrication approach that enables control over the aspect ratio, desired pattern, and dimension of silicon oxide nanowires. We further demonstrate that the technique can be used to generate various patterns of silicon oxide nanowires. The fabrication of the amorphous silicon oxide nanowires using a reactive ion plasma chamber under room temperature can be easily integrated into the manufacturing process in the electronic industry. A potential optoelectronic property of the nanowire was also investigated and the blue light photoluminescence of the as-fabricated nanowires was established. We further demonstrate the ability to directly fabricate, in a one-step approach, patterned arrays of silicon oxide nanowires when a laser interference ablation procedure is incorporated into the silicon oxide fabrication scheme.

RESULTS AND DISCUSSION

Scheme 1 shows the steps that we used to generate the silicon oxide nanowires. A silicon substrate with 5 μm thermal silicon oxide layer is coated with a thin film of PS-b-P4VP block copolymer. The asymmetric block copolymer phase separates, upon solvent annealing in a toluene/tetrahydrofuran (THF) environment, to give hexagonal vertical cylinders as shown in the atomic force microscopy (AFM) phase and topographical images in parts A and B of Figure 1, respectively. Analysis of the AFM phase and topographical contrast images gives the average domain size of the P4VP block to be ~25 nm and the average interdomain spacing to be ~40 nm. Iron metal-loading of the phase-separated block copolymer was achieved by dipping the substrate in a 1 wt % iron salt solution in hydrochloric acid for 2 min. This was then followed by a rigorous rinse in distilled water as shown in Scheme 1C. Dipping the substrate in the iron salt solution results in the preferential complexation of iron to the P4VP component of the PS-b-P4VP phase-separated block copolymer. The presence of iron in the P4VP block increases the etch resistance of the P4VP domain in comparison to the PS domain in an O_2 plasma. Using a plasma thermal reactive ion etching (RIE) tool, all organic materials are removed from the substrate leaving behind Fe_xO_y nanoparticles replicating the hexagonal ordering of the P4VP cylinders as shown in Scheme 1D. The X-ray photoelectron spectroscopy (XPS) of iron after it was loaded as a salt complex into the P4VP domain and after it was deposited as ceramic iron oxide on the silicon oxide substrate, is shown in Figure 2.

The XPS spectra in Figure 2 show the binding energies for Fe $2P_{3/2}$ and Fe $2P_{1/2}$ to be 712.5 and 726.25 eV, respectively, for iron salt present as a complex with P4VP. After RIE and the formation of Fe_xO_y ceramic nanoparticles, there is an increase in the binding energies for Fe $2P_{3/2}$ and Fe $2P_{1/2}$ to 715 and 728.25 eV, respectively. This increase in binding energy can be attributed to a change in valency or oxidation state of iron. However, the broadening of the XPS spectrum of iron after RIE is a result of the formation of several oxides of iron. Without removing the iron oxide patterned substrate from the RIE chamber, further treatment with a plasma etch using a CHF_3/O_2 gas mixture results in the formation of silicon oxide nanowire arrays. The silicon oxide nanowires formed are end-capped with iron oxide as shown in Scheme 1E. The iron oxide can be removed from the free-standing silicon oxide nanowires by a dip rinse in hydrochloric acid solution.

Scheme 1. Scheme Showing the Steps Followed for the Topdown Fabrication of Silicon Oxide Nanoforest Using a PS-b-P4VP Block Copolymer and O_2 Reactive Ion Etching

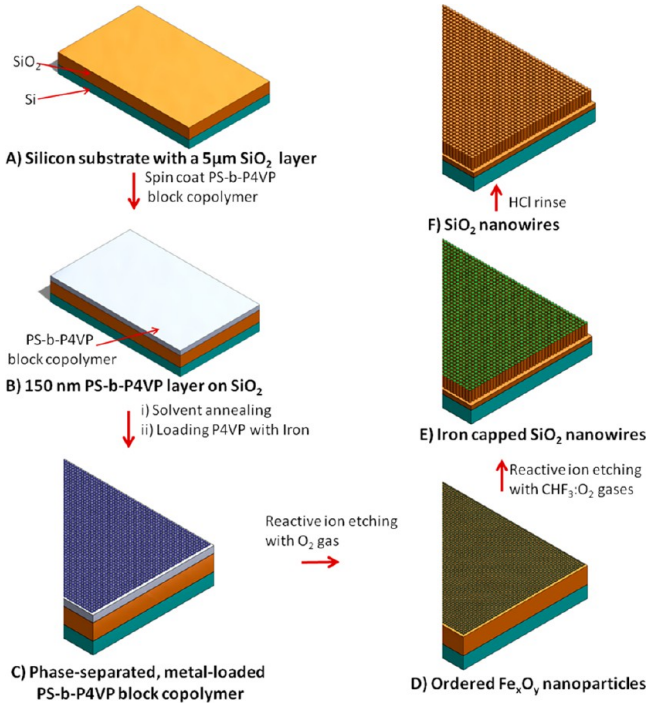

Figure 3A shows the top-down view, while Figure 3B shows the sectional view of the dense nanoforest array of silicon oxide. The nanowires shown in the SEM image have been etched for 60 min in an RIE chamber. From the sectional view, the free-standing nanowires are ~600 nm in height and vertically oriented. The nanowires appear to taper along the sides due to some degree of isotropy during the etching process. The diameter varies from 50 to 60 nm along the length of the silicon oxide nanowires, depending on the region along the length of the nanowire where the measurement is taken. The top section of the nanowires, with the iron oxide nanoparticles, has the largest diameter.

Figure 4 shows the variation in height of silicon oxide nanoforest as a function of duration of etch (mins) and demonstrates a near linear relationship between both parameters. The graph was extrapolated to the origin. After 20 min of etching the iron oxide patterned silicon oxide substrates, the resulting silicon oxide nanowires obtained are vertically oriented with no deformations or tapering along their length. The nanowires have an average diameter of 65 nm and a height of 280 nm as shown in Figure S4 in the Supporting

dx.doi.org/10.1021/am401787c | ACS Appl. Mater. Interfaces 2013, 5, 8932−8938

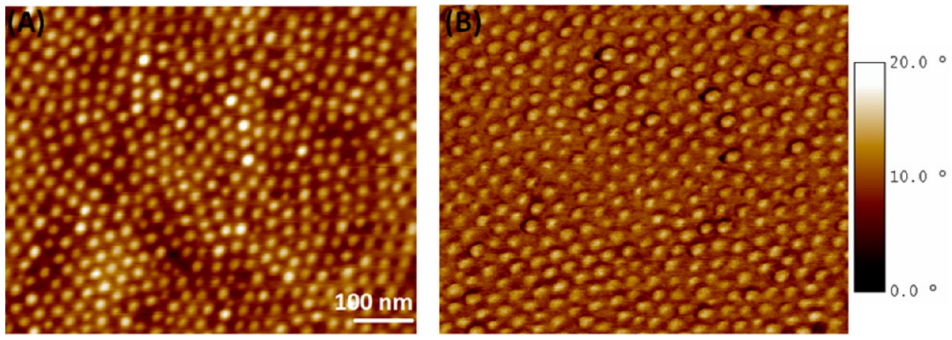

Figure 1. Atomic force microscopy (A) topographical contrast image and (B) phase contrast image of a phase separated PS-b-P4VP block copolymer showing hexagonal close packed ordering with some defects.

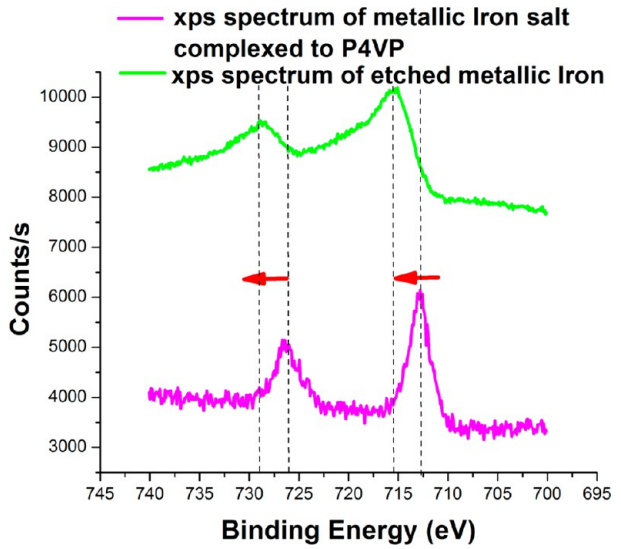

Figure 2. XPS elemental spectra of iron showing the upward shift in the binding energy of $2P_{3/2}$ and $2P_{1/2}$ after reactive ion etching in oxygen gas.

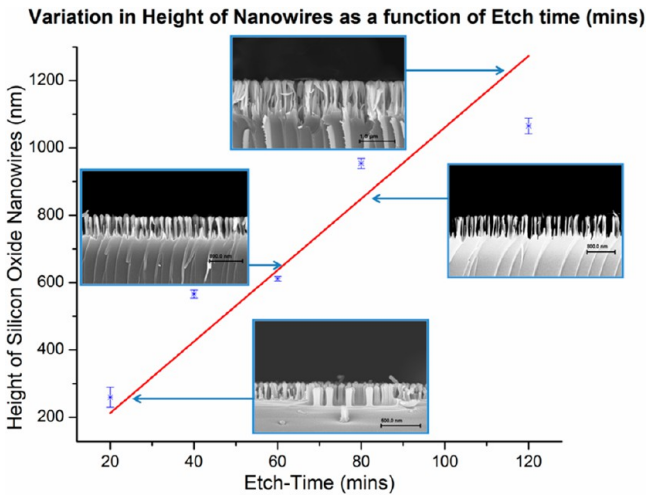

Figure 4. Graph showing a plot of height versus duration of etch (mins) for silicon oxide nanowires etched with a CHF_3/O_2 gas mixture in a plasma thermal reactive ion etching chamber.

Information. The nanowires at this stage are etched in an anisotropic etch regime with zero lateral isotropic etch from the plasma reactive gases. When the etch duration is increased to 40 min, however, the average diameter of the nanowires is found to reduce to 52 nm, while the height increases to 580 nm. There is clearly some lateral isotropic etching taking place in the chamber at this stage, and the nanowires already have kinks and deformations along their length. A further increase in the duration of etch to 60 min results in an increase in the average height of the nanowires to 600 nm and a slight reduction in the average diameter to 51 nm as shown in Figure S5 in the Supporting Information. Prolonged etch of the silicon oxide substrate in CHF_3/O_2 plasma for 120 min generates significant deformations along the length of the nanowires and some of the nanowires appear to be broken. The average diameter of the silicon oxide nanowires at this stage is still ~51 nm, but the average height of the nanowires has increased to 1 μm, as shown in Figure S7 in the Supporting Information. Figure 5A shows the high-resolution TEM image of an iron-capped silicon oxide nanowire. The diameter of the tipped portion of the nanowire, containing iron oxide, is 50 nm while

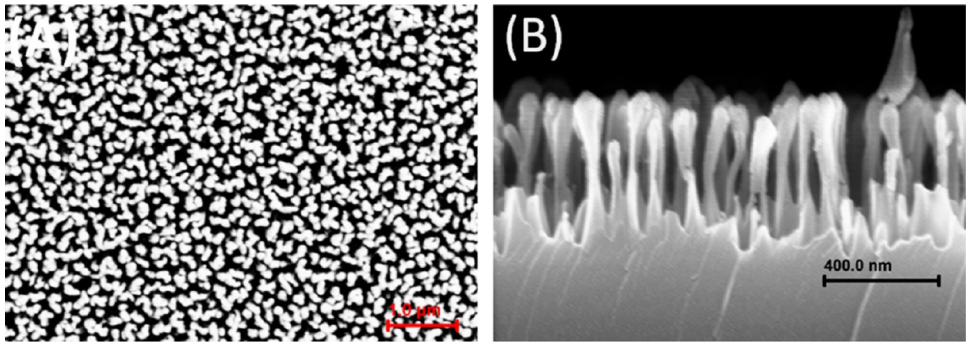

Figure 3. SEM image showing (A) top-down view and (B) sectional view of silicon oxide nanowire arrays end-capped with iron oxide.

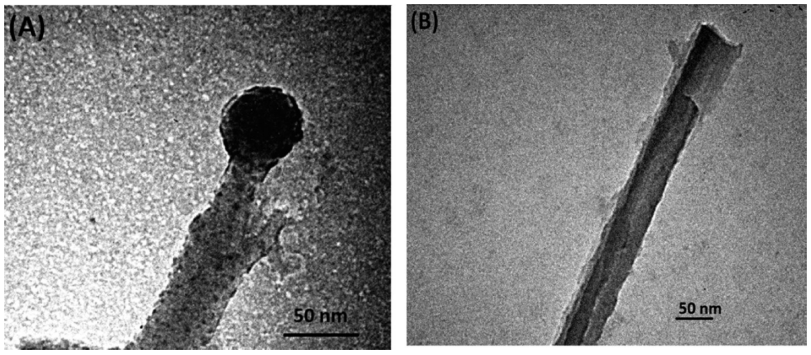

Figure 5. High-resolution TEM image of (A) iron-capped silicon oxide nanowire and (B) free-standing silicon oxide nanowire.

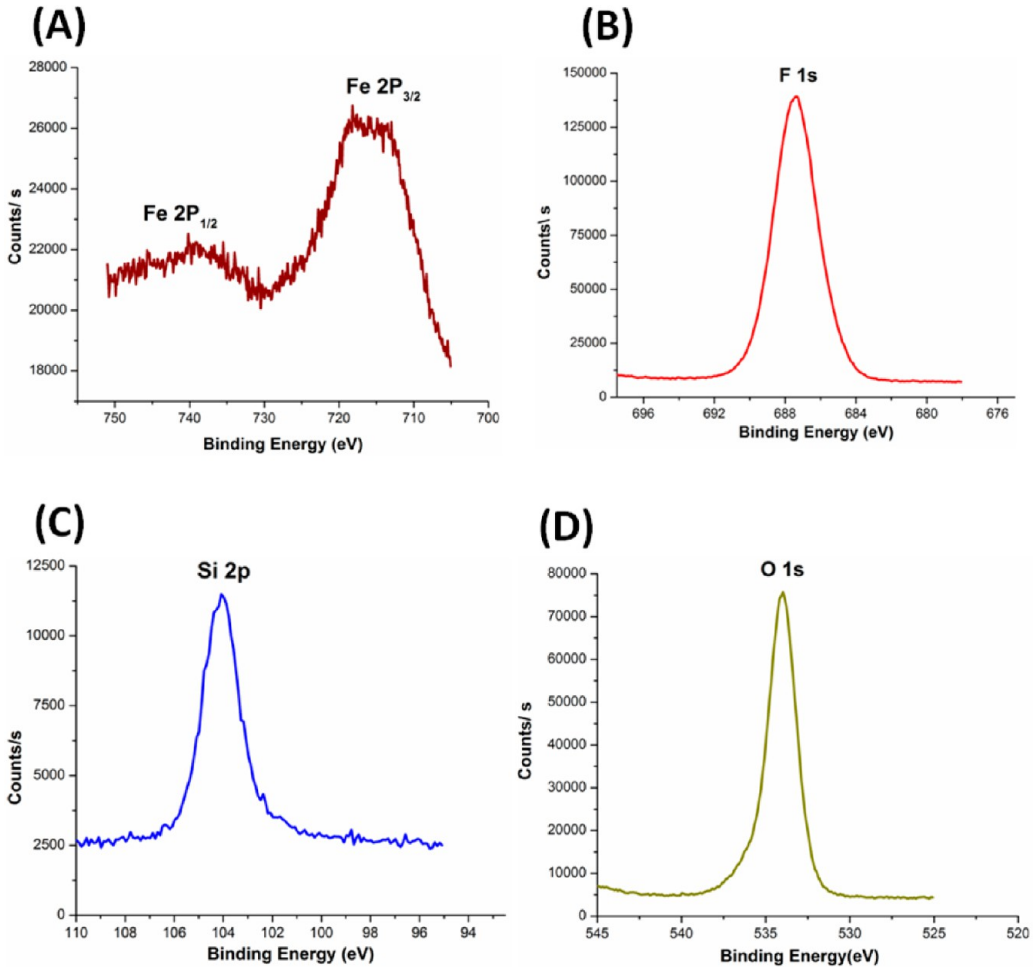

Figure 6. Elemental XPS spectra of (A) iron, (B) fluorine, (C) silicon, and (D) oxygen present in silicon oxide nanowires fabricated through plasma thermal reactive ion etching with CHF_3/O_2 gas mixtures.

the diameter of the nanowire varies along the length of the nanowire. As discussed earlier, introducing the iron oxide-capped nanowires into a hydrochloric acid solution results in the dissolution of iron oxide and generation of silicon oxide nanowires. The resulting silicon oxide nanowire after rinsing with hydrochloric acid is shown in the high-resolution TEM image of Figure 5B.

Analysis of the nanowires using XPS shows that they are composed of silicon, oxygen, iron, and doped with fluorine as shown by the XPS spectra in Figure 6A–D. Figure 6A shows the high-resolution XPS spectrum of iron with a doublet for Fe $2P_{3/2}$ and Fe $2P_{1/2}$ occurring at binding energies of 715 and 740 eV, respectively. Figure 6B shows the XPS spectrum of F 1s with a binding energy at 688 eV. The binding energy for silicon, in the silicon oxide nanowires, is increased compared to the binding energy for silicon in silicon oxide (see Figure 6C). This increase is likely due to the presence of fluorine replacing oxygen in the as-fabricated nanowires.

The binding energy of the O 1s is 535 eV (Figure 6D). The atomic composition of oxygen and fluorine from the XPS survey spectra analysis are 29% and 31%, respectively. The atomic composition of silicon was found to be 17%. The nanoscale dimensions of silicon oxide nanowires, usually results in the generation of an S band photoluminescence.

dx.doi.org/10.1021/am401787c | ACS Appl. Mater. Interfaces 2013, 5, 8932–8938

Figure 7 shows the photoluminescence spectra obtained from the as-fabricated silicon oxide nanowires with a broad blue

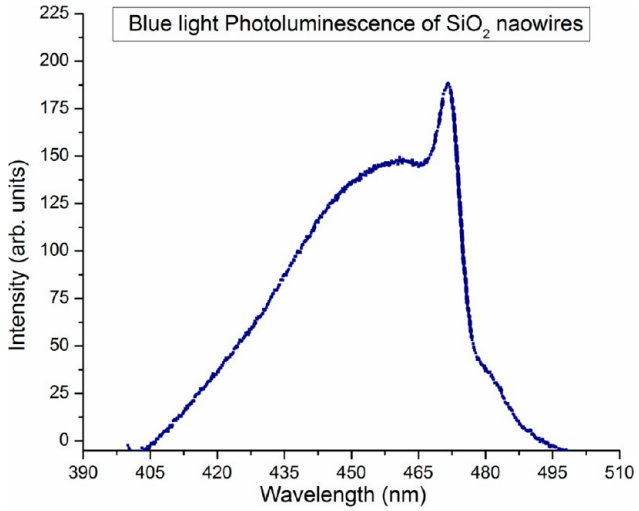

Figure 7. Photoluminescence spectra of silicon oxide nanowires end-capped with iron oxide nanoparticles at 350 nm excitation.

band luminescence peak from 430 to 475 nm. Photoluminescence measurements were performed on silicon oxide nanowires having 60 nm and 120 nm height, respectively. There appears to be no shift in the emission spectrum of the silicon oxide nanowires as a function of the height of the nanowires. Furthermore, the intensity of the photoluminescence spectrum at the blue electromagnetic wavelength region is an indication that this could be utilized for low-cost fabrication of blue light emitting devices. This luminescence behavior opens up the possibility of using this fabrication process for making optoelectronic devices as well as blue light lasers. The presence of an iron oxide-tipped section of the nanowire also opens up the possibility of using the fabrication approach for electromechanical sensors based on the parasitic-ferromagnetic property of iron oxide at room temperature. The proposed mechanism for the coalescence is shown in Scheme 2 below.

Observation using a SEM of the apparent nanoscale motion of the wires (see video available in the Supporting Information) shows that under the action of increased magnetic field the nanowires can coalesce at their tips. The PS-b-P4VP block copolymer used to fabricate the silicon oxide nanowire has been reported to be photomodifiable using a 266 nm laser interference ablation procedure.[37−39] Laser ablation of metal-loaded PS-b-P4VP block copolymer followed by RIE in O_2 plasma was used to generate hierarchical iron nanoparticles on the silicon oxide substrate. Further etching using CHF_3/O_2 plasma resulted in the generation of hierarchical arrays of silicon oxide nanowires. Figure 8A,B shows the top down and sectional SEM image of a patterned array of silicon oxide nanowires.

CONCLUSION

In conclusion we have demonstrated a new procedure for the fabrication of high aspect ratio, vertically oriented silicon oxide nanowires forming a nanoforest. The technique combines block copolymer phase separation and complexation chemistry with reactive ion etching using oxygen and CHF_3 gases. The new technique can be used to fabricate arrays of silicon oxide

Scheme 2. Schematic Showing the Mechanism for Iron-Capped Silicon Oxide Nanowire Coalescence under a Scanning Electron Microscope

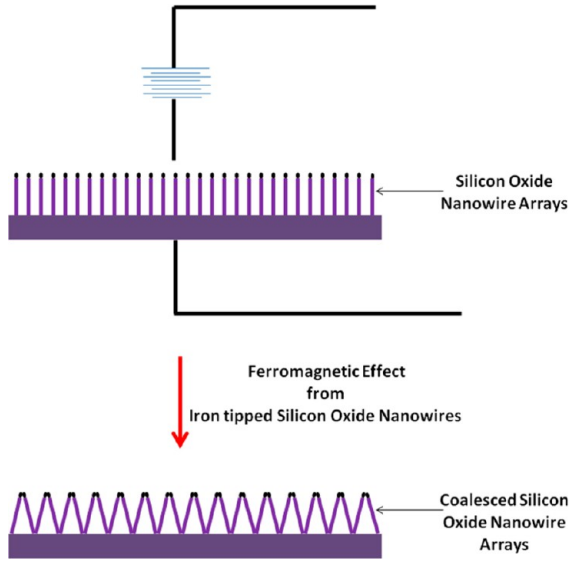

nanowires with different aspect ratios and can also be used to pattern the silicon oxide nanowires into various hierarchical designs. A potential application of the as-fabricated silicon oxide nanowire is in the fabrication optoelectronic blue light emitting devices like lasers as demonstrated by the intense blue light photoluminescence peak at 450 nm. Another potential application of the as-fabricated silicon oxide nanowire is as an electromechanical based sensor that acts when a magnetic field is present close to the nanowire arrays resulting in the coalescence of the iron-capped silicon oxide nanowire arrays.

EXPERIMENTAL SECTION

Poly(styrene-*b*-vinylpyridine) (PS-b-P4VP) block copolymer was purchased from Polymer Source Incorporated, Canada, and has weight average molecular weights (MWs) of 24 000 and 9 500 kDa for polystyrene and poly(4-vinylpyridine), respectively. The polydispersity index of the block copolymer is 1.01. Anhydrous toluene and anhydrous THF were purchased from Sigma Aldrich and used without further purification. The inorganic anhydrous iron salt, $K_3(FeCN_6)$, was purchased from Sigma Aldrich and used without further purification.

Silicon substrates with a 5 μm thermal oxide layer were purchased from University Wafers and cleaned using a piranha solution. The substrates were diced and left overnight in a piranha solution containing 70:30 vol % of H_2SO_4/H_2O_2 solution. The resulting visibly hydrophilic substrates were then rigorously rinsed in deionized water for 2 min and dried in a desiccator under nitrogen flow prior to use.

Phase Separation. Thin films of a 1 wt % PS-b-P4VP solution were prepared on cleaned silicon substrates by spin coating at 1500 rpm for 30 s, resulting in films of 150 nm thickness. This was followed by solvent annealing in a THF/toluene vapor (80:20) vol % for 5 h, leading to the generation of phase-separated vertically oriented cylinders of polyvinyl pyridine, the minor component, in a polystyrene matrix. A feature width of ∼25 nm and a periodicity of ∼40 nm was obtained after annealing.

Laser Interference Ablation. After phase separation, laser interference patterning of the block copolymer thin film was done using already published procedures.[33,34] Briefly, the 266 nm wavelength (fourth harmonic) output from a 10 ns pulsed Nd:YAG laser is split into two beams by a beam splitter. The two beams later reconverge on the phase separated block copolymer thin films, in air, forming an interference fringe. The fringe generates periodic linear

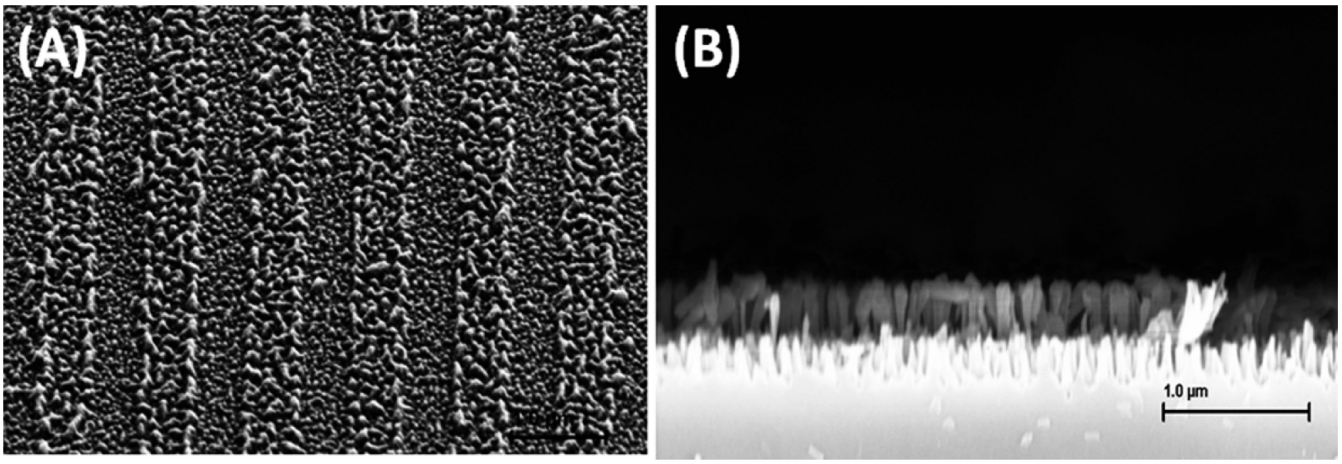

Figure 8. SEM images showing (A) top-down view and (B) sectional view of linear patterned arrays of silicon oxide nanowires end-capped with iron oxide.

regions with a localized maxima of energy dose next to regions with a localized minima of energy dose. The periodic linear intensity distribution translates into linear arrays on the phase separated block copolymer. For the generation of a square pattern, two laser interference pattern exposures with a 90° rotation of the substrate between successive shots were required.

Metal Loading of Block Copolymer. Metal loading of thin films containing phase-separated vertical cylindrical domains of P4VP was achieved by immersing thin films of the block copolymer in an 0.1 wt % solution of $K_3(FeCN_6)$ salt in 1 wt % hydrochloric acid. The hydrochloric acid activates the vinylpyridine component of the block copolymer by protonating the nucleophilic amine group in the heterocyclic ring. Hydrochloric acid also assists in the dissociation of the iron salt thus allowing complexation between the vinylpyridine and the $(FeCN)_6^-$ counterion.

Plasma Etching. Etching of the metal-loaded block copolymer thin films was done using a plasma thermal reactive ion etching (RIE) tool. The plasma reactive ion etching tool operates at a radio frequency of 13.56 MHz. Etching of the organic components was done under a pressure of 350 mTorr and a temperature of 27 °C. Oxygen flow into the RIE chamber was maintained at 50 cm^3min^{-1} and the power was set at 120W while the etch time was set for 30 min.

Silicon oxide etching was done using the same RIE tool but with CHF_3 and O_2 gases. Oxygen and trifloromethane flow rates were maintained at 5 cm^3 min^{-1} and 45 cm^3min^{-1}, respectively, while the power was set at 200 W and the pressure was maintained at 40 mTorr. The etch time for silicon oxide was varied from 20 min up to 120 min.

AFM Measurements. Phase and height images of phase separated PS-b-P4VP block copolymers were obtained using a Digital Instruments (DI) atomic force microscope (AFM) operating in the light tapping mode with a commercial silicon microcantilever tip at a resonance frequency of 360 kHz. To obtain high-resolution phase and height images, the scan rate of the AFM was set to 13 kHz.

Scanning Electron Microscope Images. Scanning electron microscopy (SEM) images were obtained using a Zeiss Ultra 60 SEM working at an acceleration voltage of 7.5 kV with a secondary electron detector. Thin film samples prior to SEM imaging were coated with gold:palladium using a Hummer gold sputterer. Sectional views were obtained by freeze-fracturing substrates having silicon oxide nanowire arrays and then imaging the sections.

Transmission Electron Microscope Images. High-resolution TEM images were obtained using a JEOL 100CX TEM operating at an acceleration voltage of 100 kV. Sample preparation for TEM involved dicing of wafers with silicon oxide nanowires and sonication of wafers in isopropyl alcohol to disperse the nanowires.

Photoluminescence Measurements. Flourescence spectra of silicon oxide nanowires were obtained using a Shimadzu fluorescent spectrometer with a Xenon arc excitation light source and an excitation wavelength of 350 nm.

■ ASSOCIATED CONTENT

Ⓢ Supporting Information

Additional SEM and TEM images of patterned as well as unpatterned arrays of silicon oxide nanowires and digital files showing the apparent coalescence of iron-capped silicon oxide nanowires under a scanning electron microscope. This material is available free of charge via the Internet at http://pubs.acs.org.

■ AUTHOR INFORMATION

Corresponding Author

*Address: George W. Woodruff School of Mechanical Engineering, 801 Ferst Drive, Georgia Institute of Technology, Atlanta, GA 30332-0405. E-mail: sumandas@gatech.edu.

Author Contributions

The manuscript was written through contributions of all authors. All authors have given approval to the final version of the manuscript.

Notes

The authors declare no competing financial interest.

■ ACKNOWLEDGMENTS

This work was funded and supported by the Defense Advanced Research Projects Agency (DARPA) Grant Number HR0011-08-0075.

■ REFERENCES

(1) Brus, L. *J. Phys. Chem.* **1994**, *98* (14), 3575−3581.
(2) Baughman, R. H.; Zakhidov, A. A.; de Heer, W. A. *Science* **2002**, *297* (5582), 787−792.
(3) Al'tshuler, B. L.; Lee, P. A. *Phys. Today* **1988**, *41* (12), 36−44.
(4) Kind, H.; Yan, H.; Messer, B.; Law, M.; Yang, P. *Adv. Mater.* **2002**, *14* (2), 158−160.
(5) Huang, M. H.; Mao, S.; Feick, H.; Yan, H.; Wu, Y.; Kind, H.; Weber, E.; Russo, R.; Yang, P. *Science* **2001**, *292* (5523), 1897−1899.
(6) Song, T.; Lee, S.-T.; Sun, B. *Nano Energy* **2012**, *1* (5), 654−673.
(7) Law, M.; Greene, L. E.; Johnson, J. C.; Saykally, R.; Yang, P. *Nat. Mater.* **2005**, *4* (6), 455−459.
(8) Atashbar, M. Z.; Banerji, D.; Singamaneni, S. *Sens. J., IEEE* **2005**, *5* (5), 792−797.
(9) Vayssieres, L. *Adv. Mater.* **2003**, *15* (5), 464−466.

(10) Wei, M.; Konishi, Y.; Zhou, H.; Sugihara, H.; Arakawa, H. *Chem. Phys. Lett.* **2004**, *400* (1−3), 231−234.
(11) Liu, B.; Boercker, J. E.; Aydil, E. S. *Nanotechnology* **2008**, *19* (50), 505604.
(12) Boercker, J. E.; Enache-Pommer, E.; Aydil, E. S. *Nanotechnology* **2008**, *19* (9), 095604.
(13) Offermans, P.; Tong, H. D.; van Rijn, C. J. M.; Merken, P.; Brongersma, S. H.; Crego-Calama, M. *Appl. Phys. Lett.* **2009**, *94* (22), 223110-3.
(14) Kodambaka, S.; Hannon, J. B.; Tromp, R. M.; Ross, F. M. *Nano Lett.* **2006**, *6* (6), 1292−1296.
(15) Cui, Y.; Lauhon, L. J.; Gudiksen, M. S.; Wang, J.; Lieber, C. M. *Appl. Phys. Lett.* **2001**, *78* (15), 2214−2216.
(16) Th, S.; Pietsch, M.; Andrä, G.; Falk, F.; Ose, E.; Christiansen, S. *Nanotechnology* **2008**, *19* (29), 295203.
(17) Woodruff, J. H.; Ratchford, J. B.; Goldthorpe, I. A.; McIntyre, P. C.; Chidsey. *Nano Lett.* **2007**, *7* (6), 1637−1642.
(18) Adhikari, H.; Marshall, A. F.; Chidsey, C. E. D.; McIntyre, P. C. *Nano Lett.* **2006**, *6* (2), 318−323.
(19) Kim, B.-S.; Koo, T.-W.; Lee, J.-H.; Kim, D. S.; Jung, Y. C.; Hwang, S. W.; Choi, B. L.; Lee, E. K.; Kim, J. M.; Whang, D. *Nano Lett.* **2009**, *9* (2), 864−869.
(20) Zheng, B.; Wu, Y.; Yang, P.; Liu, J. *Adv. Mater.* **2002**, *14* (2), 122−124.
(21) Hu, P. A.; Liu, Y. Q.; Wang, X. B. *Appl. Phys. A: Mater. Sci. Process.* **2003**, *77* (6), 743.
(22) Wang, F.; Malac, M.; Egerton, R. F.; Meldrum, A.; Li, P.; Freeman, M. R.; Veinot, J. G. C. *J. Phys. Chem. C* **2007**, *111* (5), 1865−1867.
(23) Kong, J.; Franklin, N. R.; Zhou, C.; Chapline, M. G.; Peng, S.; Cho, K.; Dai, H. *Science* **2000**, *287* (5453), 622−625.
(24) Wang, J.; Gudiksen, M. S.; Duan, X.; Cui, Y.; Lieber, C. M. *Science* **2001**, *293* (5534), 1455−1457.
(25) Duan, X.; Huang, Y.; Cui, Y.; Wang, J.; Lieber, C. M. *Nature* **2001**, *409* (6816), 66−69.
(26) Uchino, T.; Kurumoto, N.; Sagawa, N. *Phys. Rev. B* **2006**, *73* (23), 233203.
(27) Duan, X.; Lieber, C. M. *Adv. Mater.* **2000**, *12* (4), 298−302.
(28) Jiang, Z.; Xie, T.; Yuan, X. Y.; Geng, B. Y.; Wu, G. S.; Wang, G. Z.; Meng, G. W.; Zhang, L. D. *Appl. Phys. A: Mater. Sci. Process.* **2005**, *81* (3), 477−479.
(29) Ni, H.; Li, X.; Gao, H. *Appl. Phys. Lett.* **2006**, *88* (4), 043108-3.
(30) Liu, K.; Feng, Q.; Yang, Y.; Zhang, G.; Ou, L.; Lu, Y. *J. Non-Cryst. Solids* **2007**, *353* (16−17), 1534−1539.
(31) Li, X. X.; Tang, Y. H.; Lin, L. W.; Li, J. L. *Microporous Mesoporous Mater.* **2008**, *111* (1−3), 591−595.
(32) Chen, P.; Xie, S.; Ren, N.; Zhang, Y.; Dong, A.; Chen, Y.; Tang, Y. *J. Am. Chem. Soc.* **2006**, *128* (5), 1470−1471.
(33) Chang, S.-W.; Chuang, V. P.; Boles, S. T.; Ross, C. A.; Thompson, C. V. *Adv. Funct. Mater.* **2009**, *19* (15), 2495−2500.
(34) Bang, B. M.; Kim, H.; Lee, J.-P.; Cho, J.; Park, S. *Energy Environ. Sci.* **2011**, *4* (9), 3395−3399.
(35) Gay, G.; Baron, T.; Agraffeil, C.; Salhi, B.; Chevolleau, T.; Cunge, G.; Grampeix, H.; Tortai, J. H.; Martin, F.; Jalaguier, E.; Salvo, B. D. *Nanotechnology* **2010**, *21* (43), 435301.
(36) Ghoshal, T.; Senthamaraikannan, R.; Shaw, M. T.; Holmes, J. D.; Morris, M. A. *Nanoscale* **2012**, *4* (24), 7743−7750.
(37) Alabi, T. R.; Yuan, D.; Das, S. *MRS Online Proc. Libr.* **2012**, *1412*, 1.
(38) Alabi, T. R.; Yuan, D.; Das, S. *MRS Online Proc. Libr.* **2012**, *1412*, 1.
(39) Alabi, T. R.; Yuan, D.; Das, S. *Nanoscale* **2013**, *5*, 3912−3917.